



HAL
open science

Characterisation of the surface damage of X38CrMoV5 (AISI H11) tool steel at room temperature and 600 degrees C

M. Shah, Catherine Mabru, Farhad Rezai-Aria

► **To cite this version:**

M. Shah, Catherine Mabru, Farhad Rezai-Aria. Characterisation of the surface damage of X38CrMoV5 (AISI H11) tool steel at room temperature and 600 degrees C. *Fatigue and Fracture of Engineering Materials and Structures*, 2015, 38 (6), p. 742-754. 10.1111/ffe.12280 . hal-01611089

HAL Id: hal-01611089

<https://hal.science/hal-01611089>

Submitted on 7 Nov 2018

HAL is a multi-disciplinary open access archive for the deposit and dissemination of scientific research documents, whether they are published or not. The documents may come from teaching and research institutions in France or abroad, or from public or private research centers.

L'archive ouverte pluridisciplinaire **HAL**, est destinée au dépôt et à la diffusion de documents scientifiques de niveau recherche, publiés ou non, émanant des établissements d'enseignement et de recherche français ou étrangers, des laboratoires publics ou privés.

Characterisation of the surface damage of X38CrMoV5 (AISI H11) tool steel at room temperature and 600 °C

M. SHAH^{1,3}, C. MABRU² and F. REZAI-ARIA¹

¹Université de Toulouse, INSA, UPS, Mines Albi, ISAE; ICA (Institut Clément Ader), Route de Tiellet, Campus Jarlard, Albi, France, ²Université de Toulouse, INSA, UPS, EMAC, ISAE; ICA (Institut Clément Ader), 10 Av. Edouard Belin, Toulouse Cedex 4, France, ³Mechanical Engineering Department, University of Engineering and Technology, Taxila, Pakistan

ABSTRACT A novel approach is used to characterise the surface damage of AISI H11 hot work tool steel. The fatigue crack growth rate (FCGR) experiments on thin specimens, considered representative of the surface of tool steels, are carried out. Single edge notched tension specimens of 8 mm width and different thicknesses are used in the study. Initially, the effect of thickness (scale) on the FCGR is investigated to establish if there exists a difference between bulk and near surface properties of the tool steel. Then, the effect of R value on the thin specimens is investigated. All the experiments are carried out at room temperature and 600 °C. These temperatures represent the limits of use of this steel. Paris curves are established. Effect of R ratio on the threshold value of propagation at elevated temperatures is investigated in detail. A special ascending ΔK experiment for establishing the threshold of propagation at elevated temperatures in small specimens is proposed, and the results are presented. The increase in R ratio increases the FCGR at low temperature, while it has no effect at 600 °C. A reduction in thickness shows a reduction in the FCGR. Increase in temperature increases the FCGR and dramatically increases the threshold of crack propagation. The sharp increase in threshold value is studied in detail. Scanning electron microscopy of the specimens is performed to explain some of the characteristics observed in the specimen testing.

Keywords fatigue crack growth rate; high temperature fatigue; J-integral; R ratio; surface damage; threshold.

NOMENCLATURE

a	= crack length (mm)
C	= Paris' law constant: intercept
da/dN	= fatigue crack propagation rate (m/cycle)
e	= specimen thickness (mm)
E	= Young's modulus (GPa)
E'	= Young's modulus in plane strain (GPa)
f(a/W)	= correction factor for K_I
g(a/W)	= correction factor for $\sqrt{J_{el,pl}E'}$
J	= contour integral (J/m ²)
J _{el}	= elastic contour integral (J/m ²)
J _{el,pl}	= elastic-plastic contour integral (J/m ²)
$\sqrt{J_{el,pl}E'}$	= elastic-plastic crack driving force parameter (MPa.m ^{1/2})
K_I	= mode I stress intensity factor (MPa.m ^{1/2})
m	= Paris' law constant: Slope
R	= fatigue load ratio = (minimum stress / maximum stress)
R _{0.2}	= yield stress for 0.2% plasticity (MPa)

- R_m = maximum tensile strength (MPa)
- SEM = Scanning electron microscopy
- θ = temperature °C
- ν = Poisson's ratio
- W = specimen width (mm)

INTRODUCTION

The surface of hot forming tools undergoes severe thermo-mechanical loading as well as corrosion and oxidation due to its exposure to the environment. The damage of tool steels is principally in a thin layer of material near the surface,^{1,2} up to a depth of between 50 and 300 μm . Oxidation and thermal fatigue effects on the surface are studied in Ref. [3]. Different methods of fatigue/damage characterisation of thin specimens and layers can be found in the literature. The authors in Ref. [4–8] have studied thin films. The techniques used by these researchers, changes the microstructure completely as compared with the bulk material. Characterisation in this case consists of micro-scale and nanoscale damage. Tensile tests are carried out at room temperature on laser surface hardened H13 steels. Small specimens are machined from the bulk material containing only the modified layer up to 500 μm thickness.⁹ The effect of different coatings on the thermal fatigue behaviour is studied extensively in Ref. [10–12]. Aluminium immersion experiments with Energy Dispersive Spectroscopy (EDS) measurements around the crack were performed in Ref. [13]. Other methods are based on tribological characterisation of the

surfaces. In most of these, studies the surface microstructure is modified or is attached to the bulk material. In this study, an approach was proposed to machine a thin specimen near the surface of the material and perform fatigue crack growth rate (FCGR) experiments on this thin specimen (Fig. 1). It is considered that this thickness scale represents the scale of surface cracks in tools and dies.^{1,2,14} The machining of thin specimens ensures that the microstructure of the bulk and thin specimen is the same, as is in the case of surface of tool steels. These experimental results are then compared to draw conclusions on the FCG behaviour of specimens with low thickness. In this study, the effect of R value on different thicknesses is explored. All the experiments are carried out at room temperature and at 600 °C.

Most of the work on fatigue at elevated temperatures is carried out on nickel-based or cobalt-based super alloys. Mechanism-based fatigue life model in in-phase and out-of-phase thermo-mechanical fatigue tests have recently been proposed by R. L. Amaro *et al.*¹⁵ for the single crystal Ni-based super alloys taking into account the anisotropy of the alloy. The fracture behaviour of notched Powder Metallurgy (PM) super alloys under Low Cycle Fatigue (LCF) at 550–700 °C has been studied.¹⁶ Effect of notch tip plasticity is also discussed, which

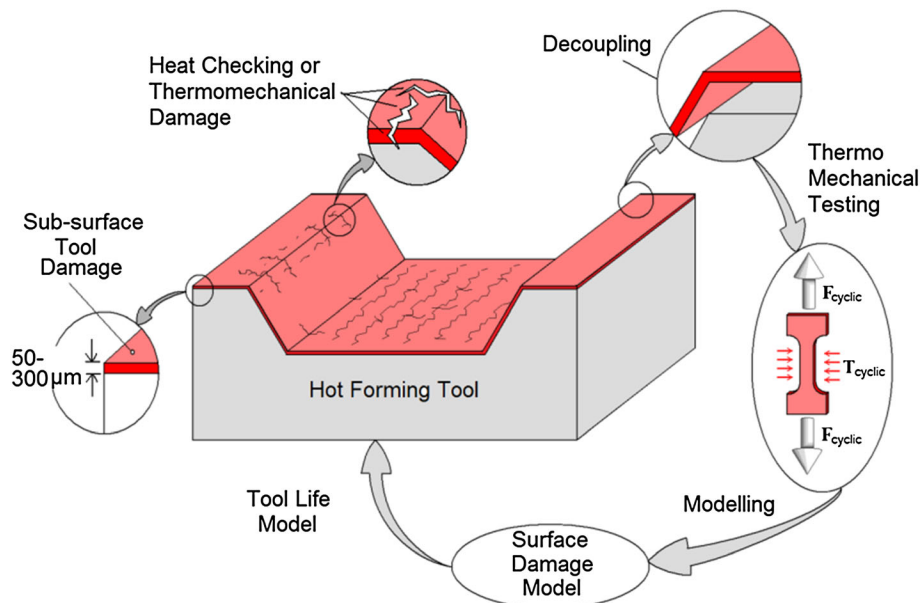


Fig. 1 Tool surface damage characterisation and modelling approach.

reduces the fatigue crack growth rate near the notch. Similar work was performed at higher temperatures of 850 °C.¹⁷ Non-local invariant method has been determined to be very effective in collapsing the different TMF data produced as a result of different notch severities and load amplitudes at 900 °C.¹⁸ Strain energy density has been used to characterise the cycles to failure in the high cycle regime of a 40CrMoV13.9 steel from room temperature up to 650 °C.¹⁹ A comprehensive treatment of the recent developments of the brittle and quasi-brittle materials tested at high temperature fatigue has been recently published.²⁰

Threshold values of FCGR at 600 °C are found to be excessive. Constraint effects of the starter notch may play an important role in this as well as the effects of thickness of the fracture toughness transferability as discussed in Refs. [21–23]. This paper does not deal with the constraint effects due to the dimensions of the notch and the specimen. Effect of high threshold values at elevated temperatures is studied in detail in this paper. Threshold value is studied at different thickness, mean stress as well as different R values of 0.1, 0.5 and 0.7. Usually a descending ΔK strategy is used to determine threshold Stress Intensity Factor (SIF) value. In this procedure, an initial pre-cracking is done on a notched specimen. Due to this pre-cracking, a plastic zone ahead of crack tip is created. Once the crack length reaches a specific length, the load is reduced (usually by 20%). Crack propagation experiment is continued until the crack length exceeds the plastic zone generated during pre-cracking. This strategy of reduction in load and subsequent propagation is continued until the desired load and crack propagation speed (threshold range) is attained. The experiment is then continued at a constant load until fracture. The procedure adopted earlier is necessary to obtain valid FCGR data of metallic materials. However, this procedure requires that the specimens have enough width so that after the reduction in load and propagation there is enough material left for the FCGR experiment. In small specimens, this is not always possible because of the small width.

A procedure of ascending ΔK is used coupled with a stepwise increase in temperature to clearly demonstrate the increase in threshold values at higher temperatures is described in this research.

This work presents an important database of the FCGR of H11 tool steel, which is currently unavailable in the literature at ambient and at elevated temperatures.

MATERIAL AND SPECIMEN PREPARATION

Experiments are carried out on a hot work martensitic tool steel X38CrMoV5 (AISI H11) delivered free of charge by Aubert & Duval in the form of forged bars of 60 mm square section. It is a low Si and low non-metallic particle content, 5% Chrome steel principally used in HPDC industry. The steel is quenched and double-tempered to a hardness of 47 HRC and $R_{0.2}$ of about 1200 MPa at room temperature. The chemical composition by weight % and the tensile properties at different temperatures are given in Table 1.

Material properties like E, R_m and $R_{0.2}$ change with temperature. The evolution of these tensile properties is shown in Table 2.

All single edge notched tension (SENT) specimens are machined by wire cut electro erosion on an Agiecut 100D wire cut machine (GF Machining Solutions, Schaffhausen, Switzerland) as in Fig. 2a. The flat surfaces of the specimens are then ground parallel to the loading axis on an LIP 515 surface grinder. In the last stage, the specimens are polished on a metallographic polisher Buehler® PHEONIX 4000 (Buehler, Dusseldorf, Germany), to obtain the final thickness with a mirror finish using a 1 μ m grit diamond paste. A grid of 0.10 \times 0.10 mm is engraved on some of the specimens as in Fig. 2b.

Crack propagation experiments were carried out on a servo hydraulic universal testing machine Walter+Bai LFV 40 (Walter+Bai, Löhningen, Switzerland). Specimens were heated to 600 °C using an induction heating system, HÜTTINGER Elektronik Axio 5 kW (TRUMPF Hüttinger GmbH + Co. KG, Freiburg, Germany), and temperature was controlled by several thermocouples. Propagation was optically observed *in situ* with a Questar® travelling microscope (1.2 μ m resolution) (Questar, New Hope, PA, USA) without interruptions. Three different thicknesses (2.5 mm, 1 mm and 0.4 mm) were tested to evaluate the effects of specimen thickness on the crack propagation behaviour at 600 °C.

Table 2 Mechanical properties at different temperatures

Temp °C	20	600
E (MPa)	208000	147000
$R_{0.2}$ (MPa)	1200	600
R_m (MPa)	1450	900

Table 1 Chemical composition of tested steel (%weight)

Elements	C	Cr	Mn	V	Ni	Mo	Si	Fe
% Mass	0.36	5.06	0.36	0.49	0.06	1.25	0.35	balance

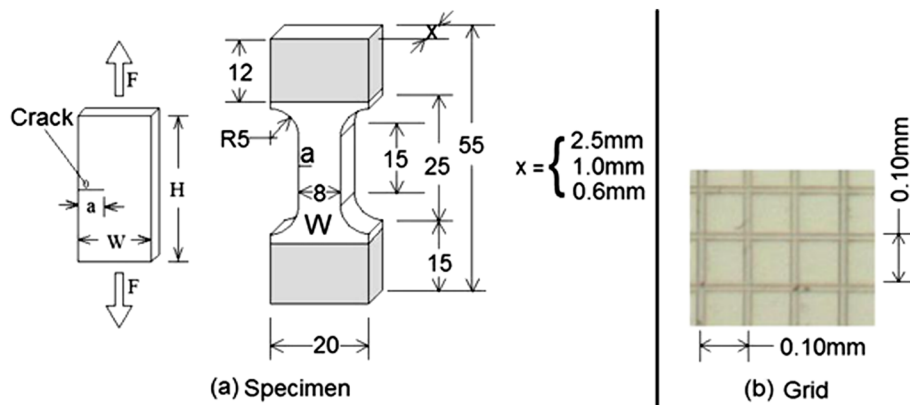


Fig. 2 (a) Specimen geometry; (b) engraved grid on specimen surface.

EXPERIMENTATION

In this section, six sets of experimental parameters are presented in sequence. Experiments are done with a view to show the effect of R ratio and specimen thickness at 25 °C and at 600 °C. The threshold fatigue at 600 °C is also explored. Details of the specimen are given earlier in Fig. 2. Results are presented in the form of Paris curves. Details of the Paris law and the SIF correction factors can be found in.^{14,24,25} Parameters of all the experiments conducted are presented in Table 3.

High temperature tests are conducted at 600 °C. High temperature grips are specially designed and manufactured for these experiments. The grip jaws are

made of IN 100, whereas the shell is made of IN 718. The grips are internally and externally water cooled, with the help of a brass jacket. The jaws are made smooth to avoid any bending or introduction of residual stresses in the thinner specimens.

CRACK DRIVING FORCE PARAMETER

One of the main concerns in a crack propagation experiment on SENT specimens is the accurate evaluation of the stress intensity factor K_I . ABAQUS® calculations (ABAQUS, Inc., Vélizy-Villacoublay Cedex - France) have been performed to determine the J-integral for

Table 3 Tests for the effects of load ratios on FCGR at different thicknesses

Group of Tests	Thickness (mm) of specimens	Applied max stress / Yield stress (%)	Load ratio R	Test frequency (Hz)	Temperature °C
1	2.5	8.3	0.1	10	25
	2.5	25	0.1		
	2.5	25	0.7		
2	0.60	25	0.1		
	0.60		0.7		
3	0.12	25	0.1		
	0.12		0.6		
4	2.50	25	0.1		
	1.00				
	0.60				
	0.25				
5	2.5	25	0.5	2	600
	2.5		0.1		
	1.0				
	0.6				
	0.6		0.7		
	0.6		0.3		
6	0.4	25	0.1	2	20 °C – 300 °C – 500 °C – 600 °C Temperature increased in steps during testing
	0.6		0.7		
	0.6				

different values of a/W , which are used to evaluate K_I using Eq. 1. An expression for correction factor $f(a/W)$ is then established by using Eq. 2. 'E' represents the Young's modulus, 'σ' applied stress, 'a' crack length and 'W' width of specimen.

$$K_I = \sqrt{J_{el} \times E(1/1 - \nu^2)} \quad (1)$$

$$K_I = f(a/W) \sigma \sqrt{\pi a} \quad (2)$$

The K_I values calculated by this procedure have been verified with the works of other researchers^{26–28} by using standard rectangular finite element models. The details of this procedure can be found in the works of Shah *et al.*^{24,29} and the expression used for the correction factor is²⁴:

$$f\left(\frac{a}{W}\right) = 1.0869 + 0.2383\left(\frac{a}{W}\right) + 1.9830\left(\frac{a}{W}\right)^2 - 2.8373\left(\frac{a}{W}\right)^3 + 2.5771\left(\frac{a}{W}\right)^4 \quad (3)$$

The details presented in²⁴ were of finite element analyses on a purely elastic material. This has been found to be sufficient for specimens at ambient temperature. However, at higher temperatures the effects of plasticity are non-negligible (SSY or small scale yielding gives way to LSY or large scale yielding), and thus the use of K_I may no longer be relevant. Use of K_I in this case may also give erroneous results on Paris curves of fatigue crack propagation.

A new crack driving force parameter $\Delta\sqrt{J_{el,pl}E'}$ was defined by Sadanada³⁰ to characterise the fatigue crack propagation of super alloys at high temperatures. The term $J_{el,pl}$ is the J-integral calculated in the finite element model by using an elastic-plastic material model. However, this parameter is a monotonic parameter and not to be confused with the cyclic J-integral of Dowling.³¹ E' is the Young's modulus for plane deformation defined as:

$$E' = E(1/1 - \nu^2) \quad (4)$$

The use of plane strain conditions in thin specimens may not represent in an accurate manner the state of stress and strain in a thin specimen. However, keeping in view the need for using a coherent and unique damage parameter for comparisons, only the plane strain condition is considered. The advantage of this parameter is that at room temperature, it gives almost the same values as for an elastic analysis because the crack tip plasticity is

very low. However, at higher temperatures this parameter shows the effects of crack tip plasticity while same dimensions (and units) as the K_I parameter. The second advantage is important for comparison of fatigue crack propagation curves at room temperature and elevated temperature. In practice the parameter takes the form²⁵:

$$\sqrt{J_{el,pl}E'} = g\left(\frac{a}{W}\right) \sigma \sqrt{\pi a} \quad (5)$$

At room temperature, the correction factor in Eq. 3 can be used because the effects of plasticity are negligible. However, the expression of the correction factor at 600 °C is presented in Eq. 6.²⁵

$$g\left(\frac{a}{W}\right) = 1.1321 + 0.0151\left(\frac{a}{W}\right) + 3.9899\left(\frac{a}{W}\right)^2 - 5.6491\left(\frac{a}{W}\right)^3 + 4.9493\left(\frac{a}{W}\right)^4 \quad (6)$$

FATIGUE CRACK PROPAGATION RESULTS

As described earlier, the six groups of test described in Table 3 are presented here in sequence in the form of Paris curves.

Effect of load ratio R at ambient temperature

Effect of load ratios in specimen of 2.5, 0.6 and 0.12 mm shows an increase in crack propagation rate with an increase in R as shown in Fig. 3(a), (b) and (c).

An interesting result is seen in the crack propagation curve of 0.60 mm specimen. The specimen tested at $R=0.7$ shows a single slope of $m=3.6$. However, the specimen tested at $R=0.1$ shows two distinct slopes of $m=3.6$ for lower ΔK values and $m=2.5$ for higher ΔK values. This effect is discussed further in the light of more results later. The increase in crack propagation speed with the increase in R value is almost five times.

The R ratio is also studied for a specimen of 0.12 mm thickness in Fig. 3(c). The R ratios selected are 0.1 and 0.6 ($R=0.7$ is not selected due to the limitations of the equipment being used for the testing procedure).

Effect of load ratio exists in all the specimens. However, it can be seen from the results earlier that the highest effect of the load ratios exists in the 0.60 mm specimens.

Effect of specimen thickness 'e' at ambient temperature

The state of stress and strain at the crack tip is dependent on the specimen thickness. American Society for Testing and Materials standards E647 and E399 impose certain

restrictions on the specimen thickness to ensure a confined plastic zone as well as plane strain conditions (thickness should be $>2.5 (KIC/\sigma_{ys})^2$). For the material

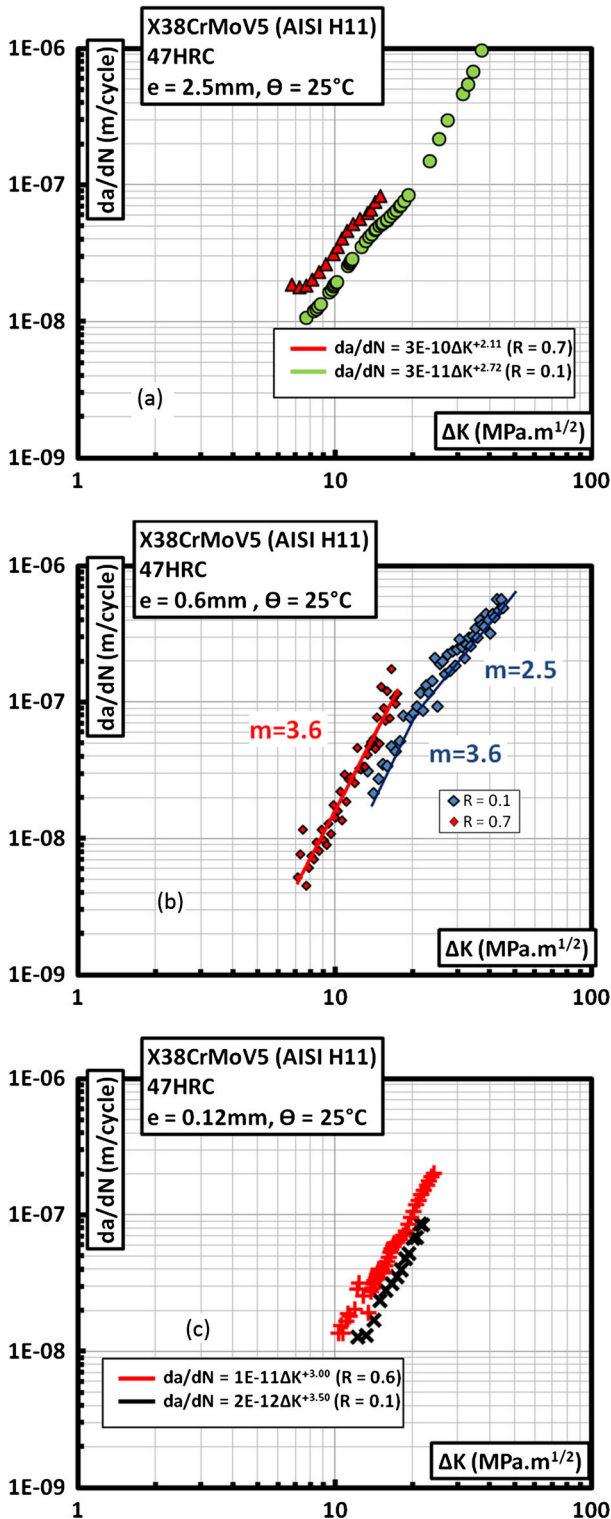


Fig. 3 (a) Effect of R ratio, comparison for 2.5 mm, (b) for 0.60 mm and (c) for 0.12 mm thickness.

used in this study, the thickness according to this criterion would be more than 15 mm. However, because this study deals with the surface and subsurface damage of the tool steels, the specimen thickness is much reduced. This is because in tool steels, the surface cracks appear in the range of 50–300 μm . The concept of using thin specimens for surface damage of tool steels has been published previously by the authors.²⁴

A comparison of FCGR of the 2.5, 0.60, 0.25 and 0.12 mm thick specimens is made in Fig. 4 at an R value of 0.1. It can be seen that the 2.5 and 0.60 mm curves coincide for lower ΔK values, however for higher ΔK ($>20\text{ MPa}\cdot\text{m}^{1/2}$), the 0.60 mm specimen shows lesser FCGR as compared with the 2.5 mm specimen. This gives this specimen its characteristic ‘Two Slope’ FCGR curve. However, it can also be seen that the thinner specimens 0.25 and 0.12 mm show slower FCGR as compared with the 2.50 mm specimen. However, the slope is parallel and unique as that of the 2.50 mm specimen.

It can be seen that the 0.60 mm specimen shows a transition thickness, where the crack tip conditions pass from the plane strain for $\Delta K < 20\text{ MPa}\cdot\text{m}^{1/2}$ (FCGR coincident with the 2.50 mm curve) to the plane stress condition for $\Delta K > 20\text{ MPa}\cdot\text{m}^{1/2}$ (FCGR coincident with the 0.25 and 0.12 mm curve). The crack propagation in thinner specimens is slower. Due to this transition from plane strain to plane stress condition, the crack propagation rate slows down during the experiment. Due to this, the FCGR curve shows an apparent reduction in the slope. This effect produces the ‘two slope’ effect witnessed in Fig. 3(b) previously.

It is expected that in the thinner specimens, the larger plastic zone creates the crack closure effect, which is eventually responsible for the reduced FCGR with a decrease in thickness.

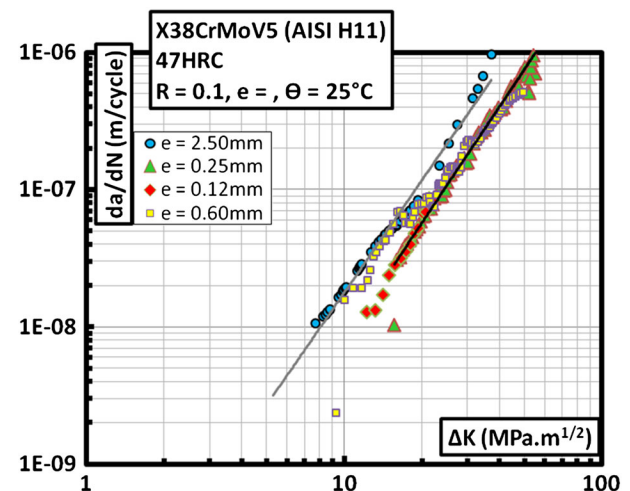


Fig. 4 Effect of thickness on FCGR at $R = 0.1$.

Effect of load ratio R at 600 °C and comparison with ambient temperature

Experiments are carried out at R=0.1 and R=0.5 for specimens of 2.5 mm thickness and R=0.1, 0.3 and 0.7 for specimens of 0.6 mm thickness. All the results of fatigue crack propagation are shown as a function of $\Delta\sqrt{J_{el,pl}E'}$. This criterion presents a better correlation between tests at 600 °C and at ambient temperature as compared with ΔK . Also, the $\Delta\sqrt{J_{el,pl}E'}$ criterion takes into account the effects of crack tip plasticity at 600 °C.

Fatigue crack propagation at 600 °C in specimens of $e=2.5$ mm at different R values seems to show absolutely no effect in the Paris region, Fig. 5(a). However, there seems to be a marked difference in the threshold values of specimens tested at different R ratios. Threshold ΔK value for R=0.1 is found to be $11.9\text{MPa}\cdot\text{m}^{1/2}$, whereas for the specimen tested at R=0.5 has a lower threshold

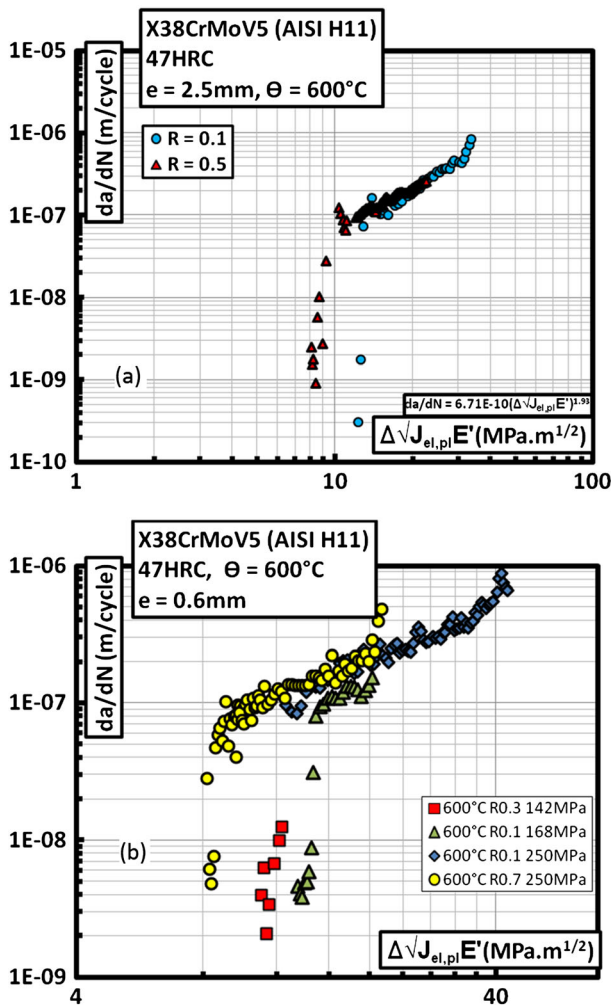


Fig. 5 (a) Effect of R ratio in 2.5 mm and (b) 0.6 mm specimen on fatigue crack propagation at 600 °C.

value of $7.8\text{MPa}\cdot\text{m}^{1/2}$. Higher crack closure in the threshold region, for R=0.1 may be the cause of this difference.

Specimens of 0.6 mm thickness have also been compared in the same manner with R=0.1, 0.3 and 0.7 in Fig. 5(b). Effect of R on the threshold value is more pronounced for 0.6 mm specimens. Threshold ΔK values are 12.8, 10.6 and $7.8\text{MPa}\cdot\text{m}^{1/2}$ for the R ratios of 0.1, 0.3 and 0.7, respectively. The increase in the threshold value of 0.6 mm specimens as compared with the 2.5 mm specimens may be due to increased plasticity in the thinner specimens (transition from plane strain to plane stress in thin specimen). This effect is graphically presented in Fig. 6.

Contrary to ambient temperature where no threshold value was detected down to $4.0\text{MPa}\cdot\text{m}^{1/2}$, ΔK_{th} clearly exists at higher loads for specimens tested at 600 °C. This could be attributed to crack closure due to crack tip plasticity at high temperature. At ambient temperature, the yield point of this metal is very high, thus the crack tip plasticity at short lengths is very insignificant. However, in a similar material, AISI 4340 heat treated to a yield strength of 1000 MPa, the threshold value has been determined at $3.0\text{MPa}\cdot\text{m}^{1/2}$ in Ref. [32]. Crack closure may also exist due to crack face mismatch. However, this mechanism exists for high a/W ratios and high ΔK , which is not the case at loads corresponding to ΔK_{th} .

Fatigue crack propagation curves for 600 °C are compared with those at ambient temperature. Figure 7(a) shows this comparison for 2.5 mm specimens with elastic and elastic-plastic crack propagation criteria, respectively. The crack propagation rate for the specimens at 600 °C is higher for low values of $\Delta\sqrt{J_{el,pl}E'}$. However, this difference diminishes for higher $\Delta\sqrt{J_{el,pl}E'}$.

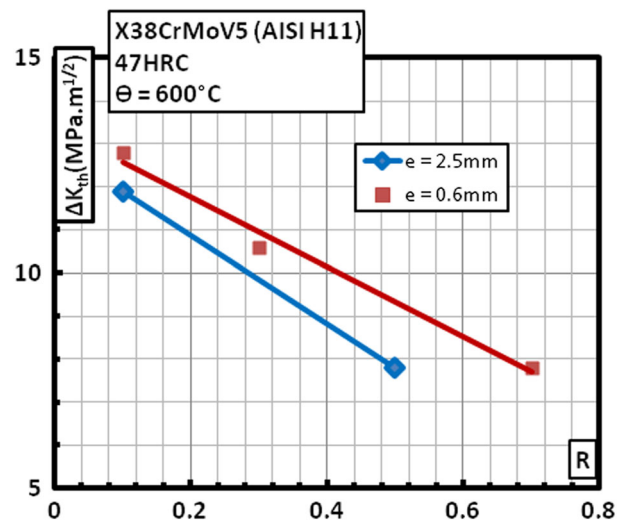


Fig. 6 ΔK_{th} as a function of load ratio R for different specimen thicknesses tested at 600 °C.

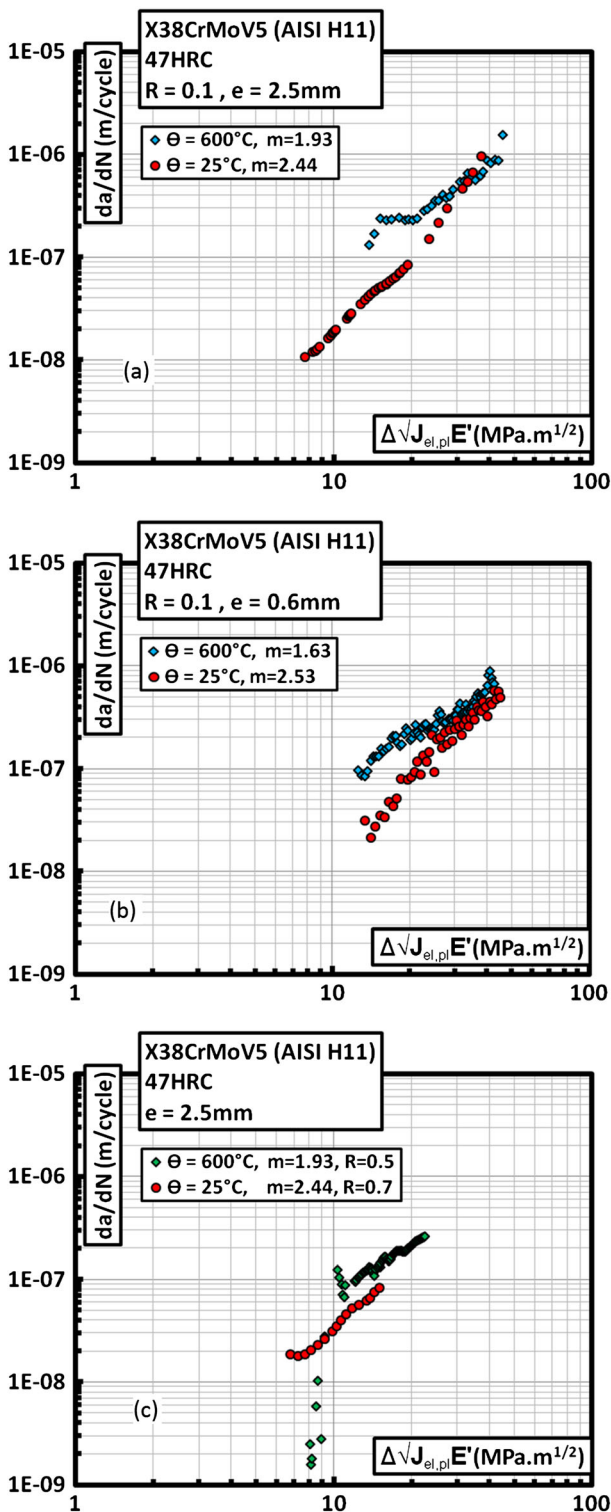


Fig. 7 Fatigue crack propagation at ambient temperature and 600 °C; (a) $e = 2.5$ mm, $R = 0.1$, (b) $e = 0.6$ mm, $R = 0.1$ and (c) $e = 2.5$ mm, $R = 0.5, 0.7$.

Specimens of 0.6 mm tested at these temperatures as shown in Fig. 7(b) show the same behaviour. The difference of fatigue crack propagation rate can be described for low, intermediate and high $\Delta\sqrt{J_{el,pl}E'}$ values as explained subsequently.

It is observed that in general, the material at 600 °C has higher crack propagation rate for low $\Delta\sqrt{J_{el,pl}E'}$ values. Slope of the Paris curve ‘ m ’ is lower at 600 °C; the consequence is that the curves intersect at some intermediate value of $\Delta\sqrt{J_{el,pl}E'}$.

K_c at 600 °C seems to be lower than at 25 °C, which again forces the curves to separate for higher $\Delta\sqrt{J_{el,pl}E'}$ values. It is pertinent to mention here that due to large number of points measured in experiments carried out on specimens of 0.60 mm thickness, the raw data is presented without cubic spline smoothing techniques.

At higher R ratio, the situation is different. Curves seem to follow a more or less parallel path in the Paris regime, with the specimen at high temperature having higher fatigue crack propagation rate, Fig. 7(c).

Threshold values for high temperature specimens are explored in an experiment performed specifically for this purpose in a 0.60 mm thickness specimen for $R = 0.1$. Under normal conditions of ascending ΔK fatigue crack propagation, there is a possibility of confusing the threshold value with the notch effect. This is because at low ΔK values, the crack length is low as well, and thus there is the risk that the crack tip is still in the large residual plastic zone of the pre-cracking. The small amount of un-cracked ligament (small specimen size) renders the exit of crack tip from the plastic zone difficult. Threshold values are thus tested at different crack lengths, while keeping the evolution of ΔK_{max} limited.

Figure 8(a) shows an experiment performed to determine ΔK_{th} and its comparison with a normal ascending ΔK crack propagation experiment. Stress values indicated are the maximum stress values applied at the specimens. The effects are summarised below as:

- Threshold value in the region of 8 to 12 $MPa.m^{1/2}$ is not an effect of the notch but is reproducible at different crack lengths. This also goes to show that probably the constraint effects are not very important in this specimen.
- Increase in the R ratio tends to decrease ΔK_{th} . This indicates a presence of crack closure at the threshold region.
- Increase in the maximum stress at 600 °C seems to increase the crack propagation rate and reduce the threshold value slightly. This increase could be due

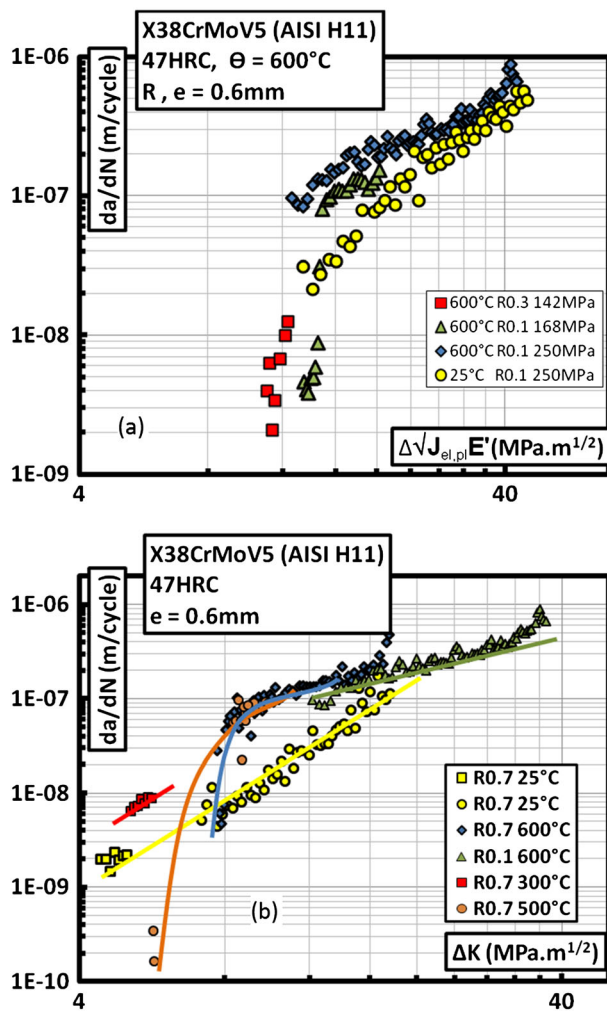


Fig. 8 (a) Determination of threshold value at elevated temperature and (b) effect of temperature variation during fatigue crack propagation. Propagation at 25 °C, 300 °C, 500 °C, 600 °C at R=0.7.

to the reduction of the effect of crack closure at higher stresses, which might also explain the apparent insensitivity of this material to R ratio when tested at 600 °C at 250 MPa.

- When compared to the specimen tested at 25 °C, it seems that the threshold values for the specimen at 600 °C is higher. In fact, no ΔK_{th} was determined for specimens at ambient temperature.

Figure 8(b) shows an experiment of increasing ΔK as well as increasing temperature to confirm the high threshold value at elevated temperatures. In this experiment, fatigue crack propagation at 25 °C is carried out in a specimen of 0.6 mm with R=0.7. An increased R gives an inherent advantage to be able to apply low ΔK values in thinner specimens more conveniently from the testing machine control standpoint. Different steps followed during the experiment and the results are listed as follows:

- 1 Fatigue crack propagation at 25 °C R=0.7. This gives a crack propagation curve that is parallel to the other FCGR curve obtained for higher ΔK values with the same loading conditions. The curve follows the simple Paris regime of propagation between 4.4 and 5.0 MPa. $m^{1/2}$. However for this level of ΔK , there is a fair amount of scattering in the FCGR data. This is shown as the yellow data in Fig. 8(b).
- 2 Specimen heated to intermediate temperature at 300 °C R=0.7. All the other testing conditions like maximum load, frequency and load ratio are kept the same. The heating is done rapidly. The fatigue crack propagation experiment is continued at 300 °C. Two distinct observations are made. One is that the FCGR increases three times, however the curve remains parallel to the FCGR curve at 25 °C (data in red in Fig. 8(b)). This may be explained by the increase in material damage with a subsequent increase in the temperature. The second observation is a strong reduction in the scattering of the FCGR data. Due to an increase in temperature, the Young's modulus decreases. This effect increases the crack opening displacement, which in turn may reduce the effects of crack face roughness and misalignment on the scattering of FCGR data. The propagation is carried out up to 5.7 MPa.m^{1/2}.
- 3 Specimen heated to 500 °C R=0.7. This temperature is 50 °C below the first tempering temperature of the material and is thus expected that no rapid phase transformation will occur at this temperature (in particular precipitation). The effects on the FCGR curve would be in principle related to mechanical properties more than metallurgical changes. However at this temperature, we find a crack arrest. It is shown as the data in brown colour in Fig. 8(b). To restart the propagation, the stress level is increased. The FCGR curve for 500 °C follows closely that of 600 °C. It should be emphasized that oxidation measurements carried out at 550 °C show a very slow oxidation rate³³ (even negligible). Therefore it can be assumed that this crack arrest effect is not related to environmental effects, but to the mechanical behaviour of the material at this temperature. The dashed black line shows the path followed up to this step.
- 4 Specimen heated to 600 °C R=0.7. Not much effect is observed on the FCGR curve, and it continues to follow the 500 °C curve. This temperature approaches the second tempering temperature of the material, so over tempering and the reduction dislocation density by thermal effects and mechanical cycling may be expected.

Experiment is continued for some increase in the crack length. Then the ΔK is reduced to try to search for the threshold value, which was the principal goal. This

value is found to be near $8 \text{ MPa}\cdot\text{m}^{1/2}$, which agrees to threshold values obtained in other experiments for these experimental conditions (Fig. 8(a) and (b)). The test is then continued up to rupture.

Results in this experiment are presented only as a function of ΔK , because the SIF correction factor for 400°C and 500°C have not been determined through numerical simulation. This experiment has established beyond any doubt that the material at high temperature of 600°C has a higher crack propagation threshold value. It has also been established that fatigue crack propagation curve for 600°C may cross over the curve for 25°C near the threshold values. The same observation was made in Ref. [34] in FCGR experiments on 18%CrNb ferritic stainless steels tested at 500°C . They have explained this effect due to plasticity-induced crack closure at 500°C as opposed to roughness-induced crack closure at room temperature. Here, the phenomenon may be explained by an increase in the crack tip plastic zone size due to reduced yield stress and drastic cyclic softening at elevated temperature. This plastic zone is large enough to cause a complete crack arrest.

Effect of specimen thickness on the fatigue crack propagation rate at 600°C and comparison with ambient temperature

Decrease in thickness favours the plane stress state condition, whereas in thick specimens, the plane strain condition prevails. This difference may have an effect on the fatigue crack propagation behaviour of the material. In this section are presented the fatigue crack propagation curves for specimens of different thicknesses all tested at 600°C .

There seems to be a trend of reduction in crack propagation rate in the Paris region with a subsequent decrease in the specimen thickness Fig. 9(a). This behaviour is less pronounced than tests carried out at ambient temperature.

The main effect however is seen at the threshold values, with those of the 0.4 mm specimen being $20.8 \text{ MPa}\cdot\text{m}^{1/2}$, which is almost twice that of the 1.0 mm and 0.6 mm specimen Fig. 9(a). Effect on the ΔK_{th} is explored in detail in the previous section. Evolution of ΔK_{th} with respect to thickness for $R=0.1$ in specimens tested at 600°C is summarised in Fig. 9(b).

MICROSCOPY

Scanning electron microscopy was carried out on the specimens in the partially cracked specimens and fully ruptured specimens to observe the crack surface. Effect of thickness reduction was in slowing down the fatigue

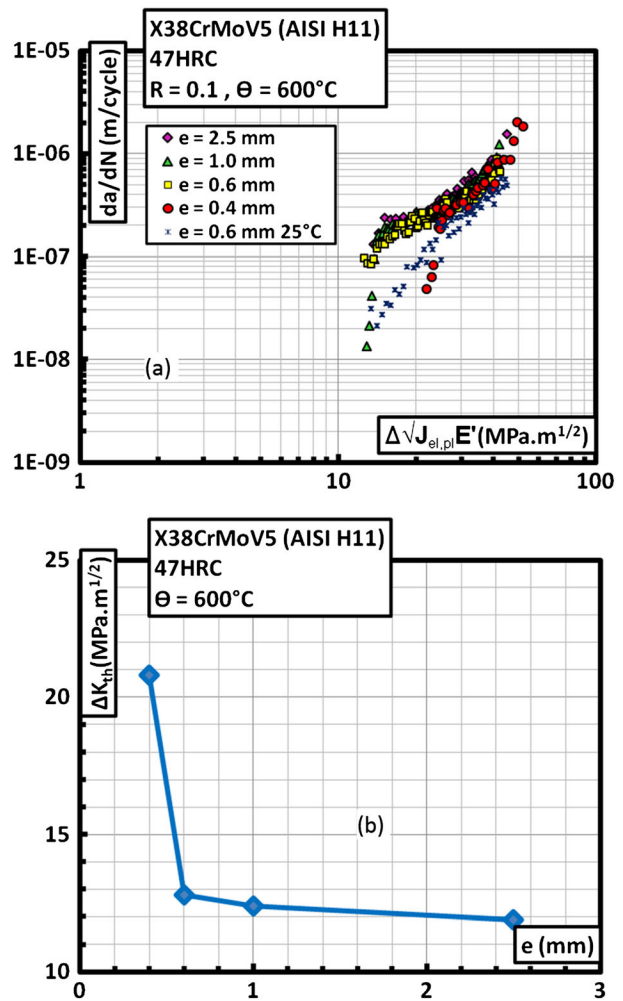


Fig. 9 (a) Effect of specimen thickness $e = 2.50, 1.0, 0.60$ & 0.40 mm at 600°C (b) ΔK_{th} as a function of specimen thickness 'e' for $R = 0.1$ tested at 600°C .

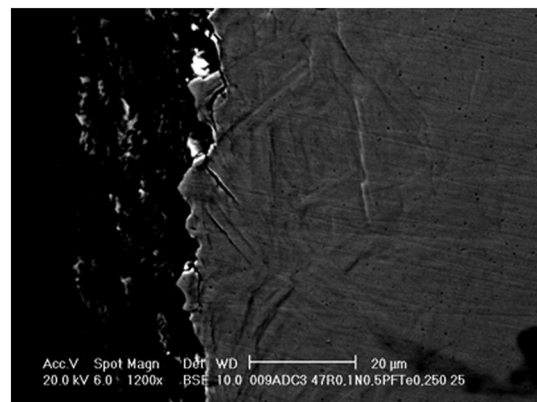


Fig. 10 Appearance of 45° inclined shear bands on the free surface in a 0.25 mm specimen.

crack growth rate. Usually, this is attributed to the increase in the plastic zone size ahead of the crack tip in thinner specimens due to plane stress conditions. This effect was clearly seen by the shear bands created ahead of the crack tip in the 0.25 mm specimen as shown in Fig. 10.

However, SEM images also show that increased plasticity causes crack closure due to crack face misalignment as shown in Fig. 11.

All these phenomena are responsible for the crack retardation in thinner specimens. Fracture surface analysis shows a flat surface in the thicker specimens of 2.5 mm and more inclined or curved surface for the thinner specimens indicating larger shear damage in thinner specimens.

Fractographic analysis of specimens tested at 600 °C shows the presence of an oxide layer with fatigue striations on the crack surface as in Fig. 12 (a). The surface consists of flat and inclined planes along the fracture

surface. Inclined planes signify the shear damage. It is of interest to note that the oxide layer is visible only on the inclined surfaces, indicating higher tendency to oxidation of the sheared surface as compared with the flat propagation area. Each plane, however, represents a completely formed crack front.

FCGR curves at 600 °C show no effect of R ratio on the propagation. This is opposite to what is observed on the crack face. Presence of oxide should increase the crack closure and hence the effect of R ratio on FCGR. Absence of this effect is explained by the process of creep. If there is creep deformation in the tension, tension fatigue test, that could explain that the two crack faces never come into contact during propagation even at a value of $R=0.1$. In one of the experiments, the partially cracked specimen was observed (nearing end of fatigue propagation), and one could clearly see the porosities created by creep deformation ahead of the crack tip as shown in Fig. 12 (b).

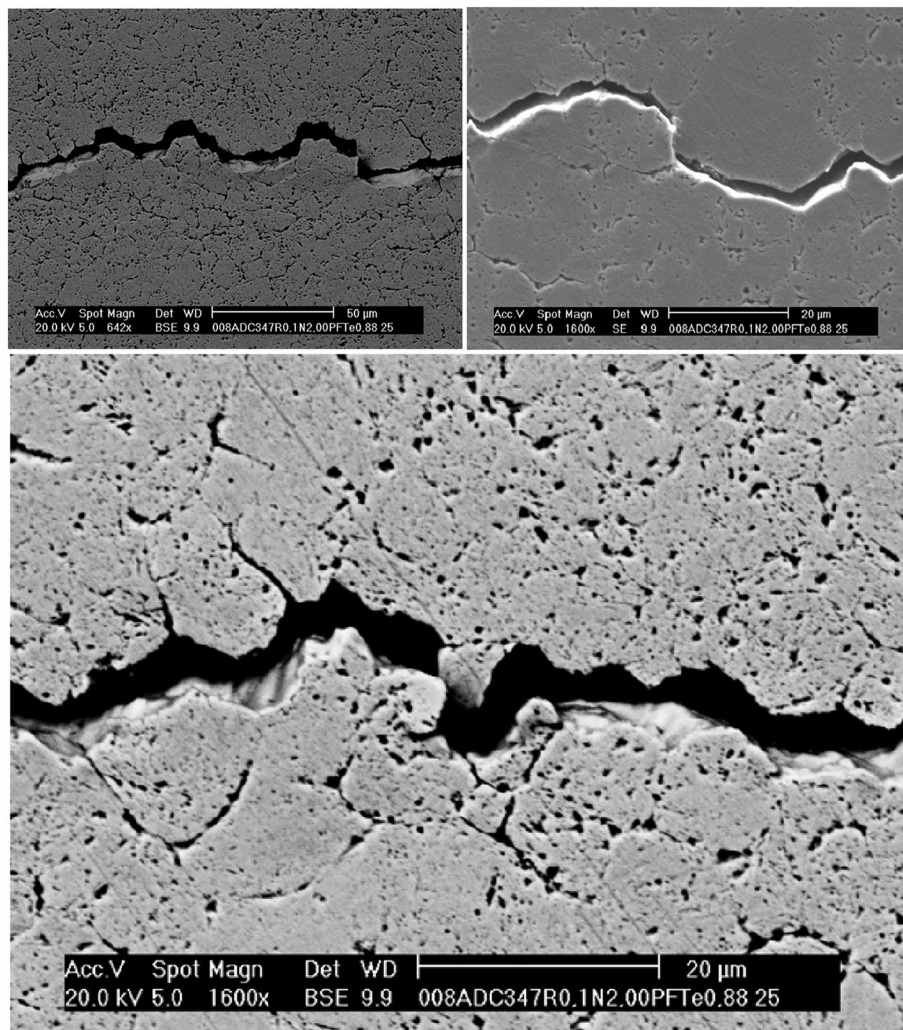


Fig. 11 Crack closure due to misalignment of crack faces and roughness of the crack faces in inter granular propagation.

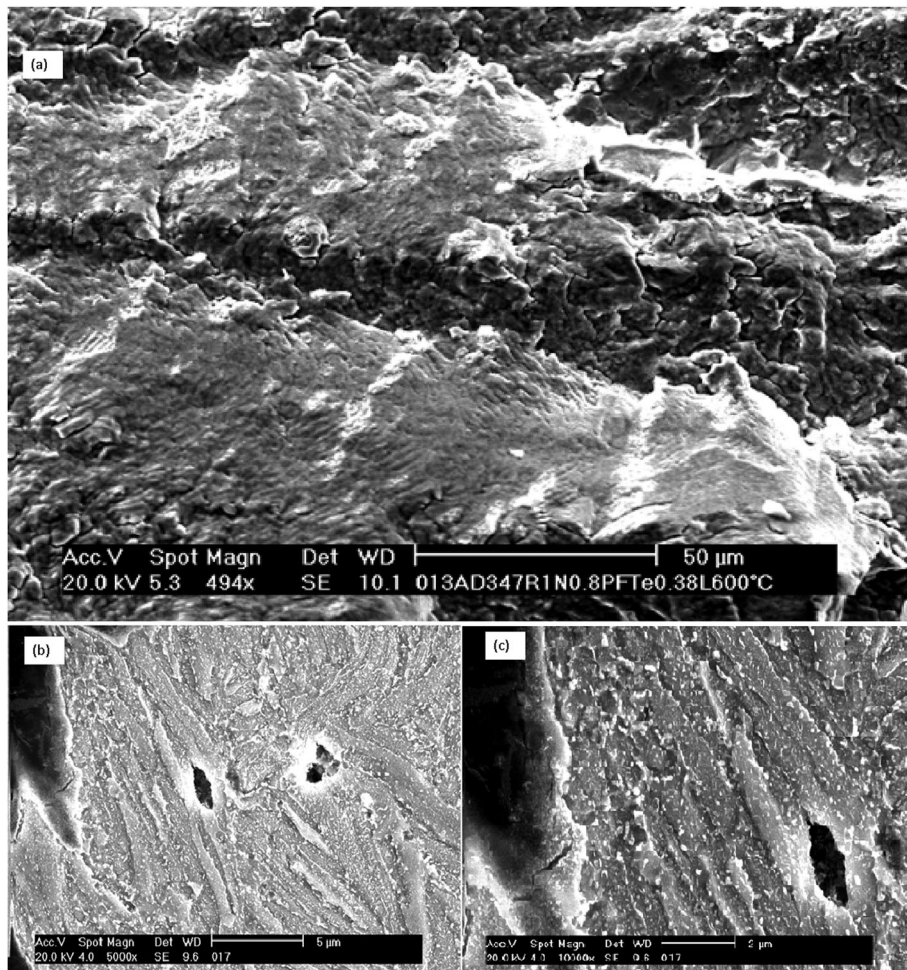


Fig. 12 (a) Multiple fully developed crack fronts in specimen tested at 600 °C and (b,c) Evidence of porosities created by creep deformation ahead of crack tip at 600 °C.

CONCLUSION

In this research, an approach to study the surface damage of tool steels is used to identify the effect of thickness on FCGR properties. Effect of load ratio 'R' value in H11 tool steel is studied. Tests are carried out at room temperature and 600 °C. These two temperatures usually represent the limits of utilisation of this tool steel. Threshold propagation at high temperatures is also deeply studied.

It is seen that at room temperature, the increase in R ratio causes an increase in the speed of crack propagation. This is usually explained by the presence of crack closure at lower R ratios. At higher temperatures, the effect of R ratio on crack propagation is different in the threshold region and the Paris region. In the stable crack regime there is almost no effect of R ratio. This is due to the absence of crack closure at elevated temperatures in this regime of propagation. However, there is a strong effect on

the threshold values. At higher R ratios the threshold values are reduced. It shows that in the threshold regime, strong crack closure effects exist. Threshold values are found to be around $12 \text{ MPa.m}^{1/2}$ for $R=0.1$ and $8 \text{ MPa.m}^{1/2}$ for $R=0.7$ at 600 °C. This effect of variation in threshold values seems to increase with a decrease in the specimen thickness. Intermediate temperature of 300 °C simply causes an increase in the crack propagation rate, but no effect on the threshold value is observed under the experimental conditions investigated. It has also been demonstrated that the threshold values are not due to stress concentration at notch or pre-cracking but an actual value. Threshold values for ambient temperature have not been established. Crack propagation is seen at SIF values as low as $3.5 \text{ MPa.m}^{1/2}$.

Effect of thickness on fatigue crack propagation has been studied. In general, it is found that the crack propagation speed is reduced with a corresponding reduction in the specimen thickness. This effect exists for both

ambient temperature and elevated temperature. However at ambient temperature, it seems that below 0.6 mm thickness, this effect diminishes. Threshold values at 600 °C seem to increase with the decrease in thickness especially for R=0.1. The reduction of specimen thickness from 0.6 mm to 0.4 mm causes a very sharp increase in ΔK_{th} .

Effect of thickness in reducing FCGR is explained using SEM micrography on partially cracked specimens. It is seen that the high plasticity ahead of the crack tip, in conjunction with crack face mismatch increases the crack closure, thereby reducing the FCGR of thinner specimens. At high temperature, the effect of R ratio is absent, even in the presence of severe oxidation. This is explained by the evidence of creep using SEM micrography.

REFERENCES

- Persson, A., Bergström, J., Burman, C. (1999) Evaluation of heat checking damage in die casting. 167–178.
- Ramous, E., Zambon, A. (1999) Dies damage in long term die casting of aluminum alloys. 179–184.
- Min, Y.-a., Jens, B., Wu X.-c., Xu, L.-p. (2013) Oxidation and thermal fatigue behaviors of two type hot work steels during thermal cycling. *J. Iron Steel Res. Int.*, **20**, 90–97.
- Schwaiger, R., Kraft, O. (1999) High cycle fatigue of thin silver films investigated by dynamic microbeam deflection. *Scripta Mater. (USA)*, **41**, 823–829.
- Kraft, O., Schwaiger, R., Wellner, P. (2001) Fatigue in thin films: lifetime and damage formation. *Mater. Sci. Eng. A*, **319**, 919–923.
- Hong, S., Weil, R. (1996) Low cycle fatigue of thin copper foils. *Thin Solid Films*, **283**, 175–181.
- Senger, J., Weygand, D., Motz, C., Gumbsch, P., Kraft, O. (2011) Aspect ratio and stochastic effects in the plasticity of uniformly loaded micrometer-sized specimens. *Acta Mater.*, **59**, 2937–2947.
- Kim, B. J., Shin, H.-A. S., Jung, S.-Y., Cho, Y., Kraft, O., Choi, I.-S., Joo, Y.-C. (2013) Crack nucleation during mechanical fatigue in thin metal films on flexible substrates. *Acta Mater.*, **61**, 3473–3481.
- Telasang, G., Dutta Majumdar, J., Padmanabham, G., Manna, I. (2014) Structure–property correlation in laser surface treated AISI H13 tool steel for improved mechanical properties. *Mater. Sci. Eng. A*, **599**, 255–267.
- Persson, A., Hogmark, S., Bergström, J. (2005) Thermal fatigue cracking of surface engineered hot work tool steels. *Surf. Coat. Technol.*, **191**, 216–227.
- Persson, A., Hogmark, S., Bergström, J. (2004) Simulation and evaluation of thermal fatigue cracking of hot work tool steels. *Int. J. Fatigue*, **26**, 1095–1107.
- Sjöström, J., Bergström, J. (2004) Thermal fatigue testing of chromium martensitic hot-work tool steel after different austenitizing treatments. *J. Mater. Process. Technol.*, **153–154**, 1089–1096.
- Klobčar, D., Kosec, L., Kosec, B., Tušek, J. (2012) Thermo fatigue cracking of die casting dies. *Eng. Fail. Anal.*, **20**, 43–53.
- Shah, M., Mabru, C., Boher, C., Le Roux, S., Rezaï-Aria, F. (2009) Crack propagation in X38CrMoV5 (AISI H11) tool steel. *TOOL 2009 - Tool steels, 02-04 June Aachen, Germany*.
- Amaro, R., Antolovich, S., Neu, R. (2012) Mechanism-based life model for out-of-phase thermomechanical fatigue in single crystal Ni-base superalloys. *Fatig. Fract. Eng. Mater. Struct.*, **35**, 658–671.
- Yuan, S., Wang, Y., Wei, D. (2014) Experimental investigation on low cycle fatigue and fracture behaviour of a notched Ni-based superalloy at elevated temperature. *Fatig. Fract. Eng. Mater. Struct.*, **37**, 1002–1012.
- Shi, D., Hu, X., Wang, J., Yu, H., Yang, X., Huang, J. (2013) Effect of notch on fatigue behaviour of a directionally solidified superalloy at high temperature. *Fatig. Fract. Eng. Mater. Struct.*, **36**, 1288–1297.
- Fernandez-Zelaia, P., Neu, R. (2014) Influence of notch severity on thermomechanical fatigue life of a directionally solidified Ni-base superalloy. *Fatig. Fract. Eng. Mater. Struct.*, **37**, 854–865.
- Berto, F., Gallo, P., Lazzarin, P. (2014) High temperature fatigue tests of un-notched and notched specimens made of 40CrMoV13. 9 steel. *Mater. Des.*, **63**, 609–619.
- Berto, F., Lazzarin, P. (2014) Recent developments in brittle and quasi-brittle failure assessment of engineering materials by means of local approaches. *Mater. Sci. Eng.: R: Rep.*, **75**, 1–48.
- Pluvinage, G., Capelle, J., Hadj Méliani, M. (2014) A review of fracture toughness transferability with constraint and stress gradient. *Fatig. Fract. Eng. Mater. Struct.*, **37**, 1165–1185.
- Matvienko, Y. G., Shlyannikov, V. N., Boychenko, N. V. (2013) In-plane and out-of-plane constraint parameters along a three-dimensional crack-front stress field under creep loading. *Fatig. Fract. Eng. Mater. Struct.*, **36**, 14–24.
- Yang, J., Wang, G. Z., Xuan, F. Z., Tu, S. T. (2013) Unified characterisation of in-plane and out-of-plane constraint based on crack-tip equivalent plastic strain. *Fatig. Fract. Eng. Mater. Struct.*, **36**, 504–514.
- Shah, M., Mabru, C., Boher, C., Leroux, S., Rezaï-Aria, F. (2009) Crack propagation in tool steel X38CrMoV5 (AISI H11) in SET specimens. *Adv. Eng. Mater.*, **11**, 746–749.
- Shah, M., Mabru, C., Rezaï-Aria, F. (2010) Investigation of crack propagation in X38CrMoV5 (AISI H11) tool steel at elevated temperatures. *Procedia Eng.*, **2**, 2045–2054.
- Chiodo, M. S., Cravero, S., Ruggieri, C. (2006) Stress intensity factors for SE (T) specimens. Technical Report BT-PNV-68, Faculty of Engineering, University of Sao Paulo .
- Cravero, S., Ruggieri, C. (2007) Estimation procedure of J-resistance curves for SE (T) fracture specimens using unloading compliance. *Eng. Fract. Mech.*, **74**, 2735–2757.
- John, R., Rigling, B. (1998) Effect of height to width ratio on K and CMOD solutions for a single edge cracked geometry with clamped ends. *Eng. Fract. Mech.*, **60**, 147–156.
- Shah, M., Mabru, C., Rezaï-Aria, F., Souki, I., Pasha, R. A. (2012) An estimation of stress intensity factor in a clamped SE (T) specimen through numerical simulation and experimental verification: case of FCGR of AISI H11 tool steel. *Acta Metall Sin (English letters)*, **25**, 307–319.
- Sadanada, S., Shahinian, P. (1980) Elastic-plastic fracture mechanics for high temperature fatigue crack growth. *Fract. Mech.: Twelfth Conference, ASTM STP*, **700**, 152–163.
- Dowling, N. E. (1976) Geometry effects and J integral approach to elastic-plastic fatigue crack growth. *ASTM Int.*, **19**, 19–32.
- Liaw, P. K., Leax, T. R., Donald, J. K. (1987) Fatigue crack growth behavior of 4340 steels. *Acta Metall.*, **35**, 1415–1432.
- Bruckel, P. (2003) Oxydation de l'Acier à Outils X38CrMoV5 à 600–700 °C et en présence de vapeur d'eau. Thesis Ecole des Mines de Paris.
- Makhlof, K., Jones, J. (1992) Near-threshold fatigue crack growth behaviour of a ferritic stainless steel at elevated temperatures. *Int. J. Fatigue*, **14**, 97–104.